Supplementary Tables

Supplementary Table 1: Primers used to clone dehydrogenase candidates from *N. mussinii* cDNA. Primers were synthesised with vector specific overhangs as described in methods. Cloned sequences NEPS2 and NEPS3 did not precisely match full length sequences contigs from the transcriptome, but appeared to contain regions from multiple contigs. The poor assembly of these genes is indicative of close paralogs or alternative splicing.

Enzyme name	SwissProt Annotation	Original contig number	Contributing contigs (after sequencing)	Gene specific primer Forward	Gene specific primer Reverse
NEPS1	Q5C9I9	c20589_g1_i1		ATG GCA AGC ACT GCA AAT CC	CTGA AGG AGC AAA GAA TGG TAA ACA AAG C
NEPS2	Q5C9I9	c20589_g2_i1	c47141_g1_i1	ATG GGC AAC AAG AAG ACG C	TGA TGT TGG TGC AAA GAA TGG T
NEPS3	Q5C9I9	c20589_g3_i1	c43881_g1_i1	ATG GCT AAC AAT TCA GTG ATG ATG AAG	TGC TGA ACC GAG GAG AAA TGG
	Q6V4H0	c21160_g1_i1		ATG GCG AAA TCA CCA GAA ACA G	GTC GGC TTT CAG TGA ACC G
	Q6V4H0	c29133_g1_i1		ATG GCG AAA TCA GTG AAC GC	ATC GGT TTC AGT CAG CGT ATT CC
	P25141	c30293_g1_i1		ATG GCC GAC AAC ACC AC	GAA CTT GAT AAT AAC CTT GAC ACA ATC AGG

Supplementary Table 2: Kinetic parameters of NEPS1 dehydrogenase activity. Activity measured spectrophotometrically by absorbance at 340 nm. Kinetic Michaelis-Menten parameters are reported as a best fit parameter estimates ± standard errors of estimated parameters with corresponding p-values.

Enzyme	Substrate	[Substrate] µM	Co-substrate	[Co-substrate] mM	Sample size n	k_{cat} s^{-1}	k_{cat} p-value	K_m µM	K_m p-value	k_{cat}/K_m s^{-1} M^{-1}
NEPS1-WT	**4a**	0.25-100	NAD^+	1	11	0.148 ± 0.002	8×10^{-14}	1.6 ± 0.1	2×10^{-7}	90000
NEPS1-WT	**4b**	1-100	NAD^+	1	11	0.32 ± 0.01	1×10^{-10}	4.9 ± 0.8	1×10^{-4}	64000
NEPS1-WT	NAD^+	1-250	**4a**	0.1	9	0.173 ± 0.003	4×10^{-10}	3.5 ± 0.3	2×10^{-5}	50000
NEPS1-T154G	**4a**	50-750	NAD^+	1	14	0.0804 ± 0.005	1×10^{-9}	251 ± 37	1×10^{-5}	300
NEPS1-T154G	NAD^+	7.8-1000	**4a**	0.5	9	0.0599 ± 0.002	4×10^{-8}	26 ± 4	7×10^{-4}	2000

Supplementary Table 3. X-ray data collection and refinement statistics

	Binary complex of NEPS3 and NAD^+ *
Data collection	
Space Group	$P2_1$
Cell dimensions (Å/°)	
a, *b*, *c* (Å)	63.92, 107.75, 69.36
α, β, γ (°)	90.0, 104.26, 90.0
Resolution (Å)	47.16 – 1.40 (1.42 – 1.40) *
R_{merge}	0.090 (1.564)
$I/\sigma(I)$	11.2 (1.2)
Completeness (%)	98.6 (97.0)
Redundancy	6.9 (6.9)
Refinement	
Resolution (Å)	47.16 – 1.40 (1.42 – 1.40)
No. reflections	167049 (8822)
R_{work}/ R_{free}	0.150/0.168 (0.276/0.283)
No. atoms	
Protein	8059
Ligand/ion	176/8
Water	1109
B-factors	
Protein	17.9
Ligand/ion	14.4/20.9
Water	30.2
R.m.s. deviations	
Bond lengths (Å)	0.011
Bond angles (°)	1.56
PDB accession code	6F9Q

*One crystal was used for this structure. *Values in parentheses are for highest-resolution shell.

Supplementary Table 4: Primers used in mutation investigation into NEPS1 and NEPS3.

Enzyme	Mutation	Forward Mutation Primer	Reverse Mutation Primer
NEPS1	N125A	GGAATTCGATAAAGTGATGCGCGTGGCCGCGCGCGGGATGGCTGC	CACGCGCATCACTTTATCGAATTCC
NEPS1	T152N	AGGAACGAGAGGCACTATTATCTGCAATACCACCCCGCTATCGTC	GCAGATAATAGTGCCTCTCGTTCCT
NEPS1	T153A	AACGAGAGGCACTATTATCTGCACGGCCACCCCGCTATCGTCGAG	CGTGCAGATAATAGTGCCTCTCGTTCC
NEPS1	T154G	CGAGAGGCACTATTATCTGCACGACCGGCCCGCTATCGTCGAGG	GGTCGTGCAGATAATAGTGCCTCTCG
NEPS1	P155S	AGGCACTATTATCTGCACGACCACCTCGCTATCGTCGAGGGGCGGGCA	GGTGGTCGTGCAGATAATAGTGCCT
NEPS1	L156S	CACTATTATCTGCACGACCACCCCGTCATCGTCGAGGGGCGGGCA	CGGGGTGGTCGTGCAGATAATAGTG
NEPS1	Y167F	GAGGGGCGGGCAAAGCATGACGGACTTTGCGATGTCGAAGCACG	GTCCGTCATGCTTTGCCCGCCCCTC
NEPS1	K171M	AAGCATGACGGACTATGCGATGTCGATGCACGCAGTGATGGG	CGACATCGCATAGTCCGTCATGCT
NEPS1	S198M	GATTAGGGTTAACTGCGTGACGCCGATGGTGGTGCTCACGCCGCT	CGGCGTCACGCAGTTAACCCTAATCC
NEPS1	V199A	TAGGGTTAACTGCGTGACGCCGTCGGCGGTGCTCACGCCGCTCG	CGACGGCGTCACGCAGTTAACCCT
NEPS1	T202A	CTGCGTGACGCCGTCGGTGGTGCTCGCGCCGCTCGCCCAACGGATG	GAGCACCACCGACGGCGTCACGCAG
NEPS1	TT152NA	AGGAACGAGAGGCACTATTATCTGCAATGCCACCCCGCTATCGTC	GCAGATAATAGTGCCTCTCGTTCCT
NEPS1	TTT152 NAG	AGGAACGAGAGGCACTATTATCTGCAACGCCGGCCCGCTATCGTC	GCAGATAATAGTGCCTCTCGTTCCT
NEPS1	TTTP152 NAGS	AGGAACGAGAGGCACTATTATCTGCAACGCCGGTAGCCTATCGTCGAGG	GCAGATAATAGTGCCTCTCGTTCCT
NEPS1	TTTPL152 NAGSS	AGGAACGAGAGGCACTATTATCTGCAACGCCGGTAGCTCATCGTCGAGG	GCAGATAATAGTGCCTCTCGTTCCT
NEPS3	N150T	GGGAAGGGGAGGGTCCATCATATGCACCGCCGGCTCGTCGGCGGT	GCATATGATGGACCCTCCCCTTCC
NEPS3	A151T	AAGGGGAGGGTCCATCATATGCAACACCGGCTCGTCGGCGGTGAG	GTTGCATATGATGGACCCTCCCCTT
NEPS3	G152T	GGGAGGGTCCATCATATGCAACGCCACCTCGTCGGCGGTGAGG	GGCGTTGCATATGATGGACCCTCC
NEPS3	S153P	AGGGTCCATCATATGCAACGCCGGCCCGTCGGCGGTGAGGGGCGCGCA	GCCGGCGTTGCATATGATGGACCCT
NEPS3	S154L	GTCCATCATATGCAACGCCGGCTCGCTGGCGGTGAGGGGCGCGCA	CGAGCCGGCGTTGCATATGATGGAC
NEPS3	Y165F	GAGGGGCGCGCATGGCGTGACGGACTTCGTGATGTCGAAGCATGC	GTCCGTCACGCCATGCGCGCCCCTC
NEPS3	K169M	TGGCGTGACGGACTACGTGATGTCGAUGCATGCGGTGATAGGGCTGGTG	CGACATCACGTAGTCCGTCACGCCA
NEPS3	M196S	TATTAGGGTTAACAGCGTGTCGCCGAGTGCCGTGGCGACGCCGCT	CGGCGACACGCTGTTAACCCTAATACTG

Supplementary Figures

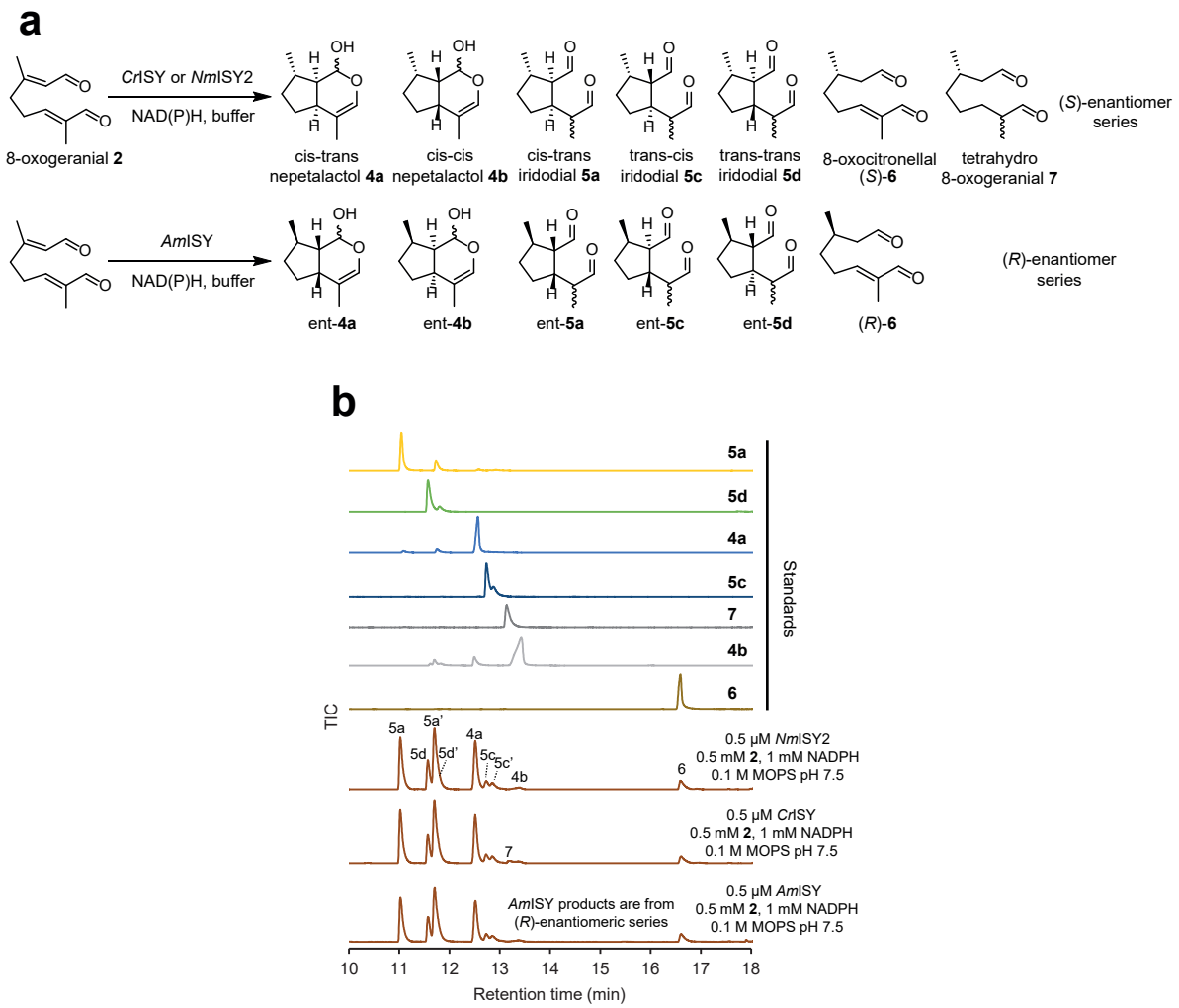

Supplementary Figure 1: 8-oxogeranial **2** reduction catalysed by ISYs from *Antirrhinum majus* (*Am*ISY), *Catharanthus roseus* (*Cr*ISY) and *N. mussinii* (*Nm*ISY2). **a**, Product structures formed in reactions. All products are isomeric and the product of a single enzyme catalysed reduction of **2** except for **7** which is formed via two reductions. **b**, GC-MS total ion chromatograms (TICs) of enzyme catalysed reductions. The product profiles obtained with all enzymes is nearly identical with respect to the diastereoselectivity of the reaction, despite the enzymes' sequence identities (48-65%) and different enantioselectivity. See Supplementary Fig. 2 for electron ionisation (EI) spectra for compound identification. The experiment was repeated independently using five different buffer concentrations (Supplementary Fig. 3) and similar results were obtained in all cases. The results are replicates of data presented in previous publications: Kries, H. et al. *J. Biol. Chem.* **292**, 14659–14667 (2017) and Sherden, N.H. et al. *Phytochemistry* **145**, 48–56 (2018).

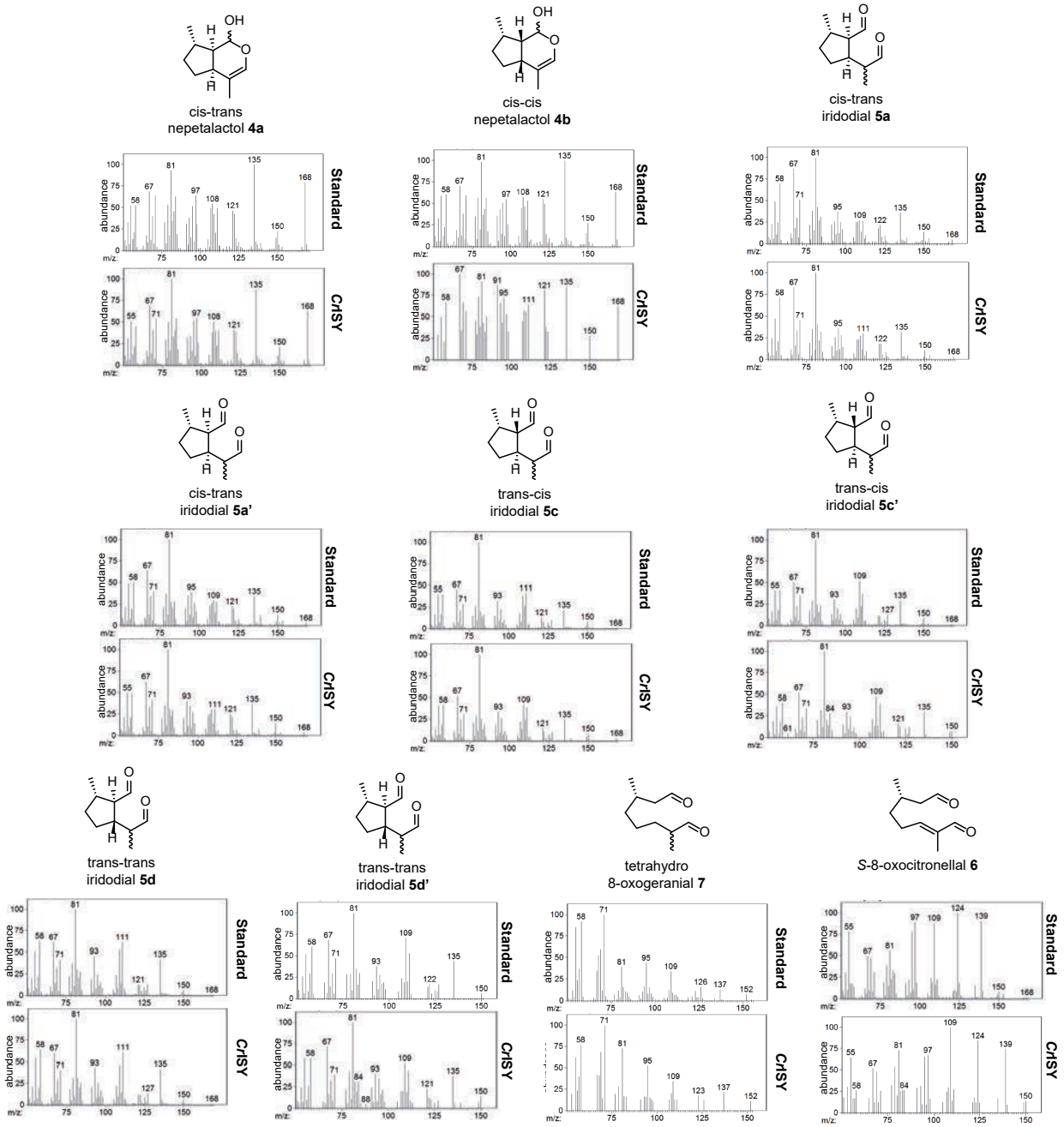

Supplementary Figure 2: Electron ionisation (EI) spectra of compounds from Supplementary Fig. 1b. All spectra were obtained from the centre of the peaks, except for the *Cr*ISY **5d'** spectrum which was taken from the peak tail to avoid overlap with **5a'**.

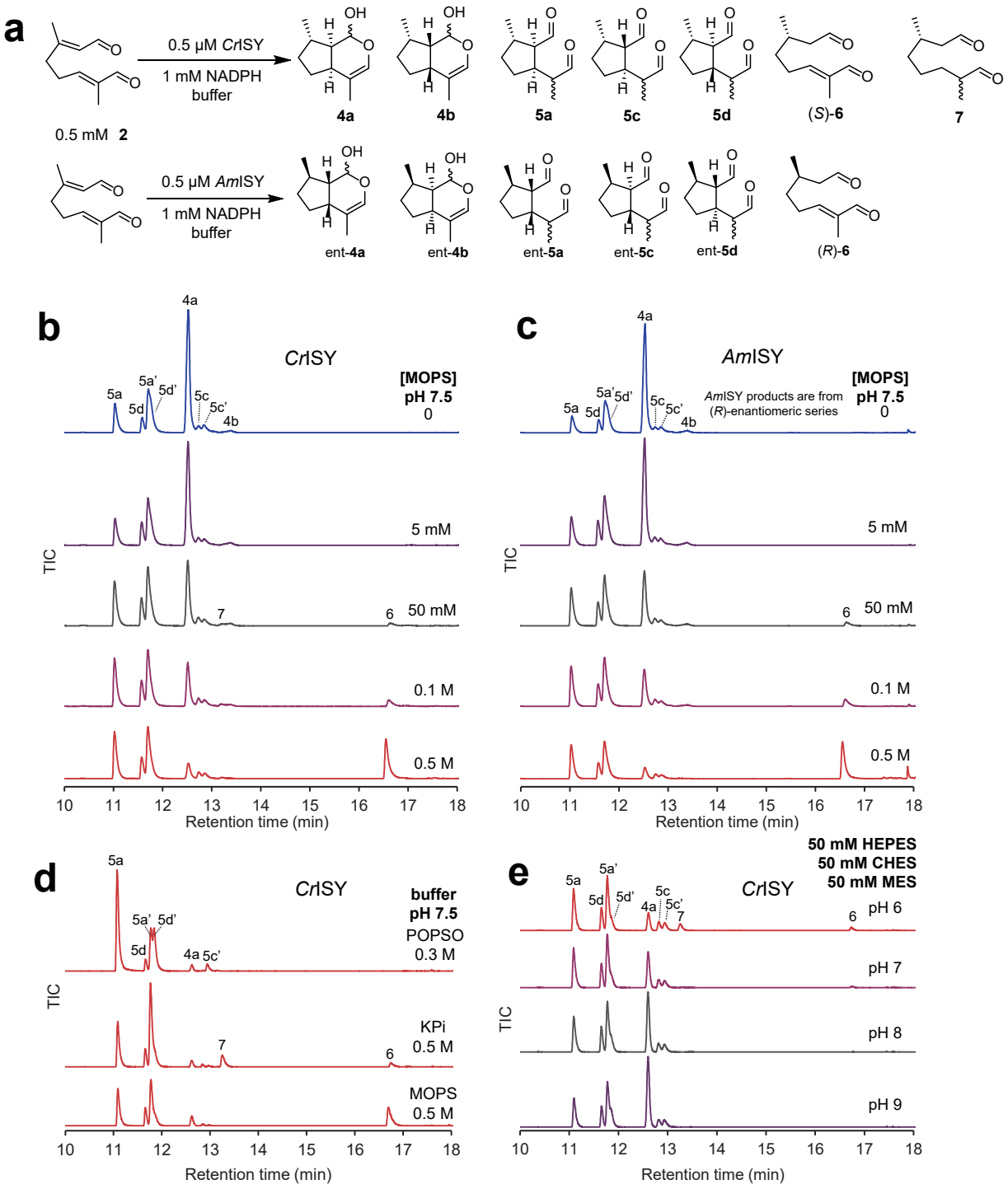

Supplementary Figure 3: Influence of buffer on ISY catalysed reduction of **2**. **a**, Reduction of **2** by *Cr*ISY and *Am*ISY. **b**, Reduction of **2** with *Cr*ISY at different MOPS pH 7.5 concentrations. **c**, Reduction of **2** with *Am*ISY at different MOPS pH 7.5 concentrations. **d**, Reduction of **2** with *Cr*ISY with different buffers. Note the different product profiles; this indicates direct involvement of buffer in the tautomerisation mechanisms. **e**, Effect of pH on product profile of *Cr*ISY catalysed reduction of **2**. Reducing the pH (more acidic) has a similar result to increasing buffer (general acid) concentrations. The experiments presented in panels b and c were repeated but employing different conditions: varying the ISY (three different ISYs, Fig. 2b, Supplementary Fig. 3) and varying the buffer (four different buffers, Supplementary Fig. 4). Similar results were obtained for all seven experiments testing buffer concentration effects. The experiments in panel d was repeated at different buffer concentrations (Supplementary Fig. 4) and similar results were observed. The experiments in panel e were repeated twice with similar results.

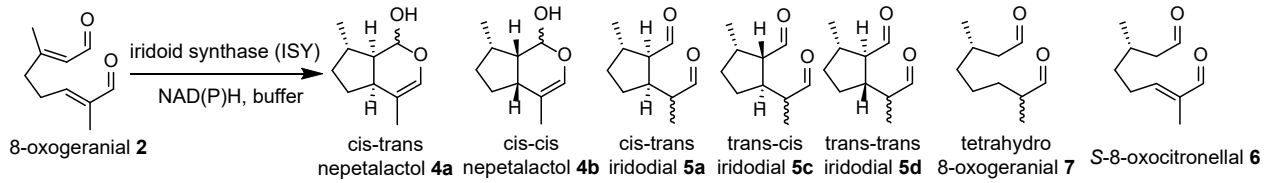

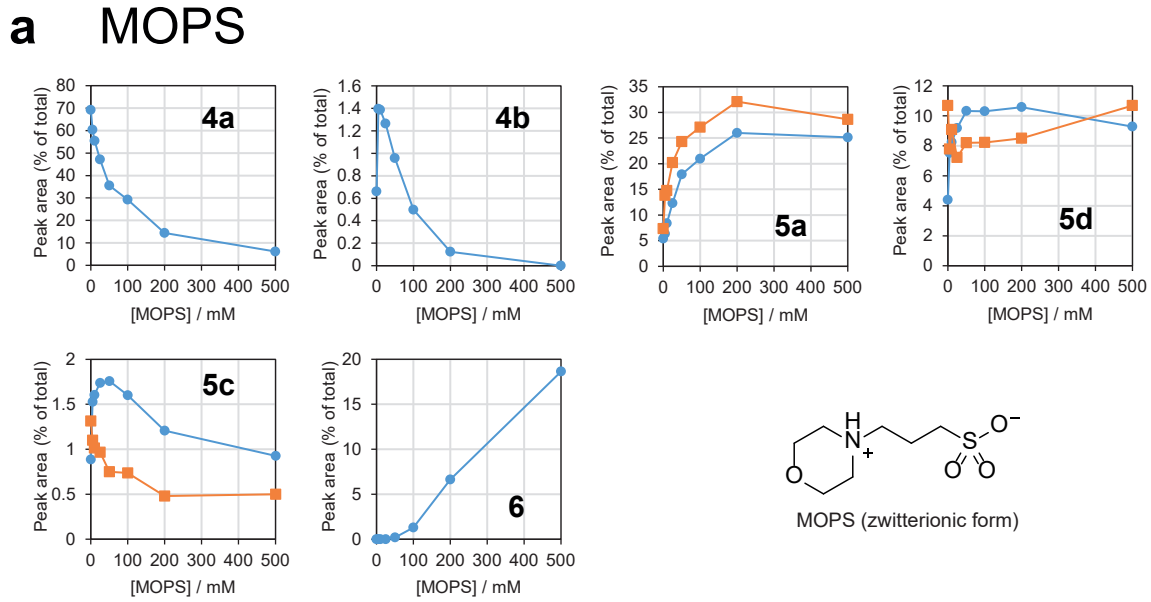

Supplementary Figure 4: Analysis of buffer influence on the ISY catalysed reduction of **2**. The reduction of **2** by *Cr*ISY was performed with different buffers at different buffer concentrations, at pH 7.5. **a**, MOPS (3-(N-morpholino)propanesulfonic acid); **b**, HEPES (4-(2-hydroxyethyl)-1-piperazineethanesulfonic acid); **c**, KPi (potassium phosphate); **d**, POPSO (Piperazine-1,4-bis(2-hydroxypropanesulfonic acid)). In all cases concentration of **4a** decreases as buffer concentration increases. Between 0-100 mM buffer concentrations of **5a** increase. Above 100 mM buffer the effects are more buffer dependent, indicating direct buffer involvement in cyclisation/tautomerisation processes. Product quantities are represented as percentage product proportions, obtained by dividing product TIC peak area by total product peak areas. Product peak areas are not normalised by standard curves so do not represent absolute concentrations. Note that peaks of **5a'** and **5d'** overlap in the GC method—peak areas for these compounds were measured as a split peak (i.e. both to baseline) and not as a peak shoulder.

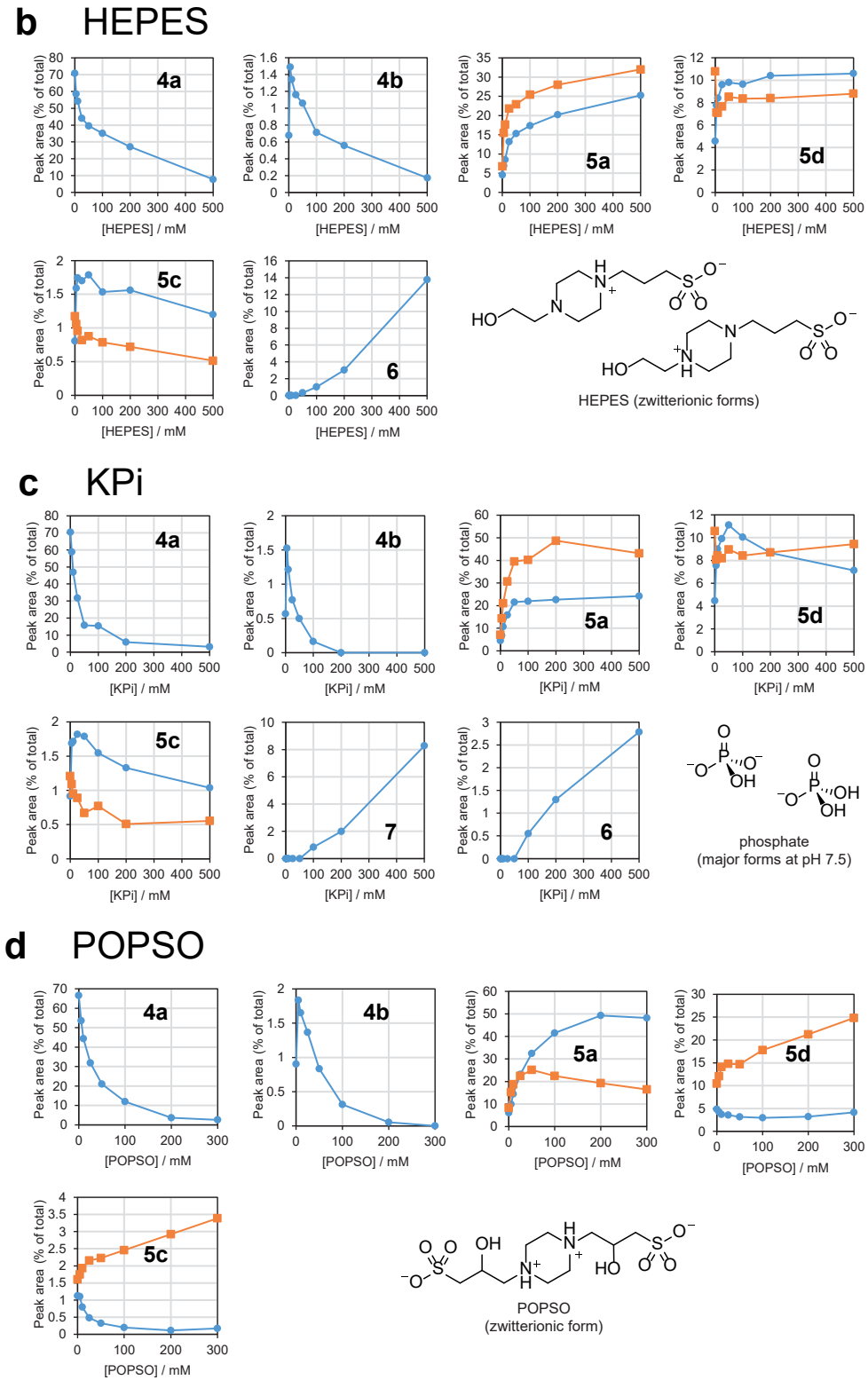

Supplementary Figure 4: continued

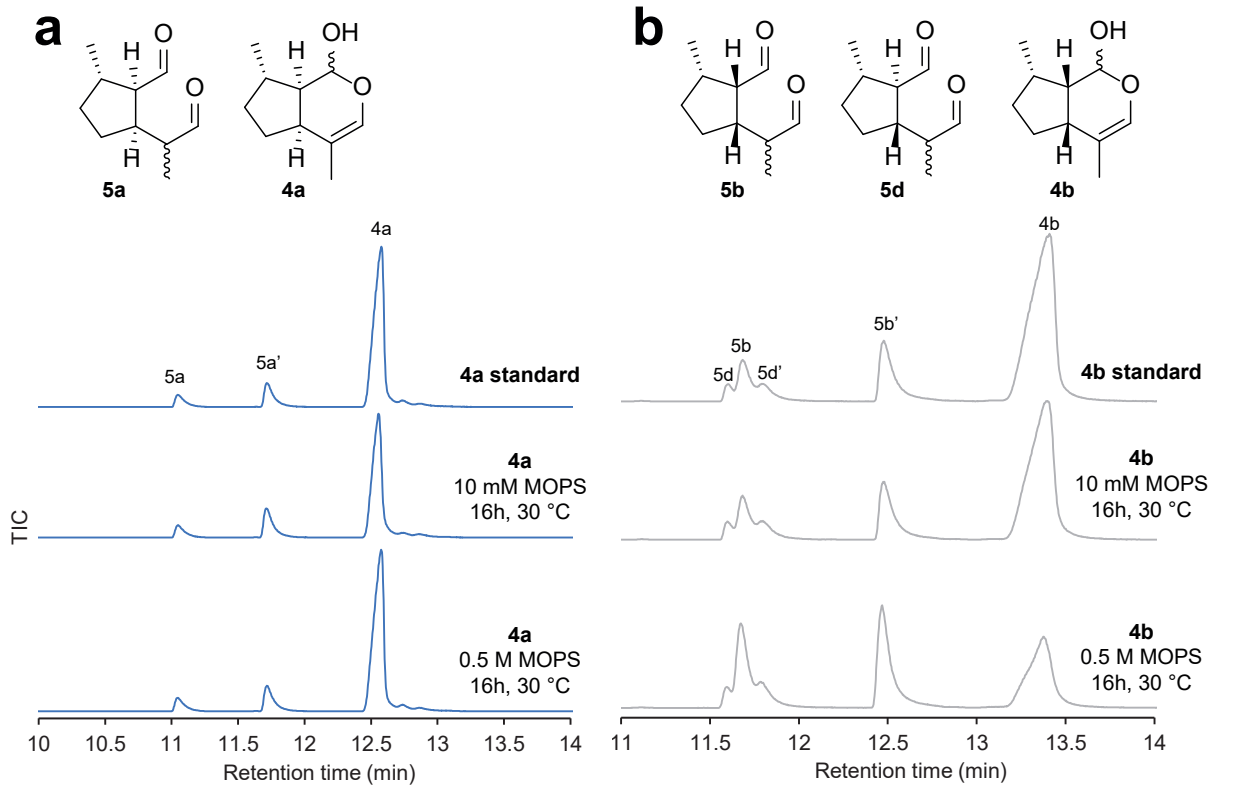

Supplementary Figure 5: Nepetalactol stability in buffer. Cis-trans-nepetalactol (**4a**, panel a) and cis-cis-nepetalactol (**4b**, panel b) stability in 10 mM and 0.5 M MOPS pH 7.5. **4a** appears to be stable in both these conditions. **4b** appears mostly stable in 10 mM MOPS pH 7.5, but is not stable in high buffer concentrations (0.5 M MOPS pH 7.5) and degrades to form iridodials **5**. The experiment in panel a was performed independently twice with similar results; the experiment in panel b was performed once.

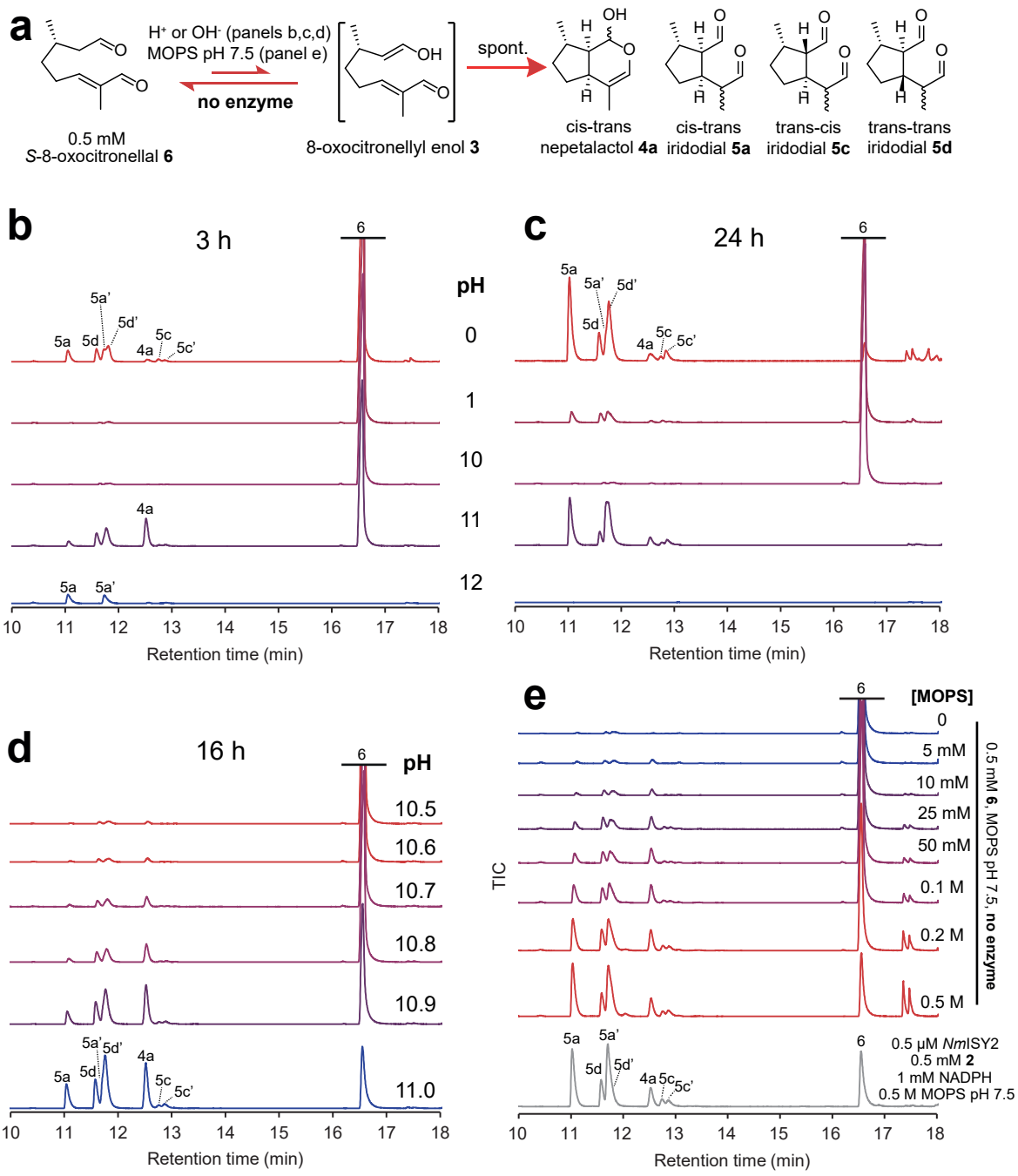

Supplementary Figure 6: Spontaneous cyclisation of *S*-8-oxocitronellal **6**. **a**, Outline of cyclisation reactions. **b**, Incubation of **6** in water at acidic (HCl) or alkaline (NaOH) pH for 3 h. No conversions were observed for samples at pH 2-9. **c**, As in panel b but after 24 h. Between pH 2-10 very little conversion was observed. Samples at pH 12 appeared to show complete degradation of **6** and products. No **4b** was detected at any pH. **d**, Incubation (16 h) of **6** in water between pH 10.5 and 11.0 (NaOH). Samples pH 10.0-10.5 demonstrated little conversion. It is notable that **4b** is absent from these spontaneous reactions. **e**, Buffer catalysed cyclisation of **6**. Non-enzymatic formation of **4a** and **5** achieved via tautomerisation and spontaneous cyclisation catalysed by buffer, presumably acting as a general acid. The product profile at 0.5 M buffer mimics the equivalent ISY catalysed reduction, supporting a non-enzyme catalysed cyclisation. See Supplementary Fig. 7 for EI spectra. The experiments in panels b-d were performed once. The experiments in panel e were performed independently twice with similar results.

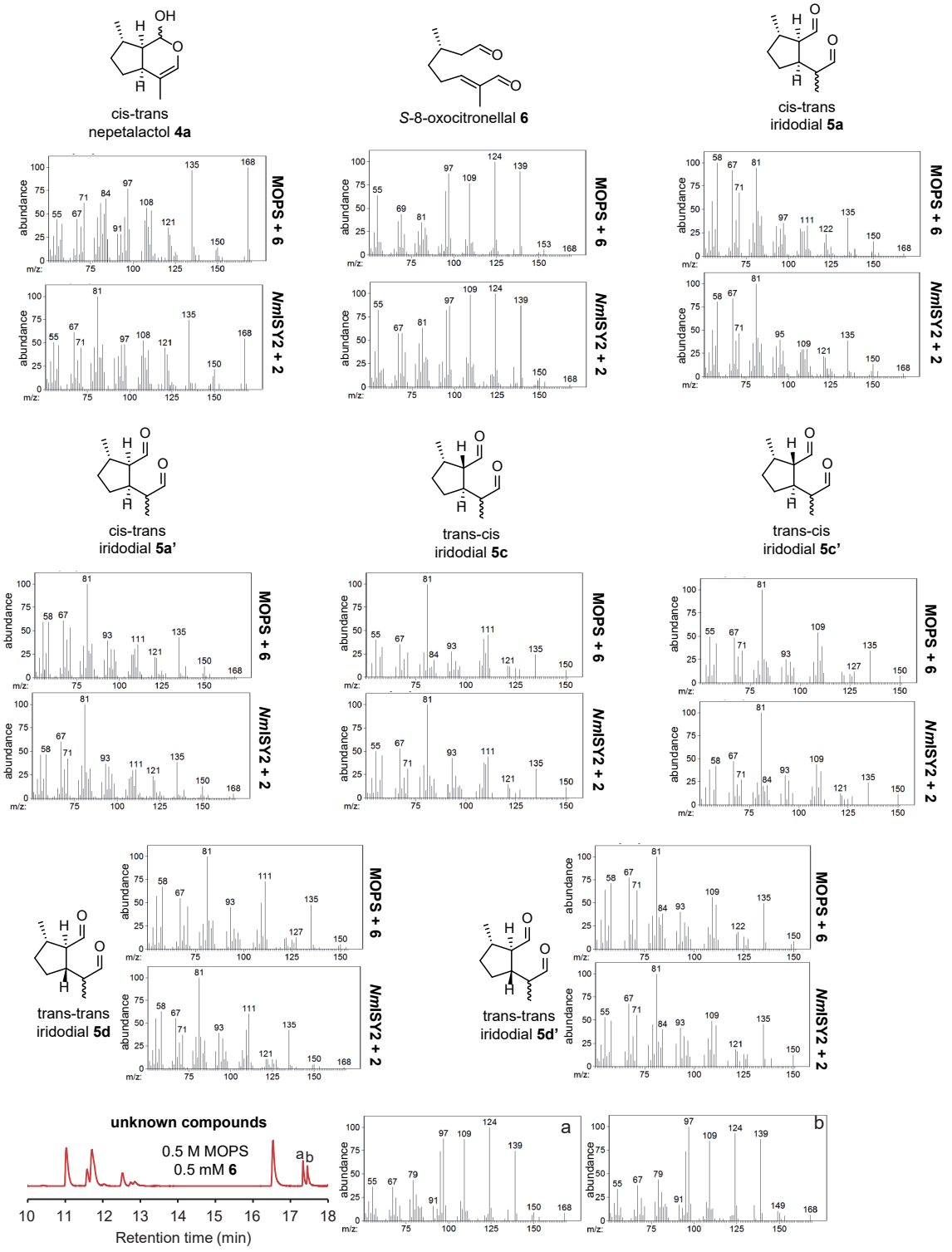

Supplementary Figure 7: Comparison of EI spectra from Supplementary Fig. 6e, bottom two TICs at 0.5 M MOPS. The spectra verify the products are chemically identical despite their different origins. Spectra of two unknown compounds produced in the non-enzymatic reactions are included; these appear to be non-cyclic isomers of **6**. All spectra were obtained from the centre of the peaks, except for the **5d'** spectra which were taken from the peak tail to avoid overlap with **5a'**.

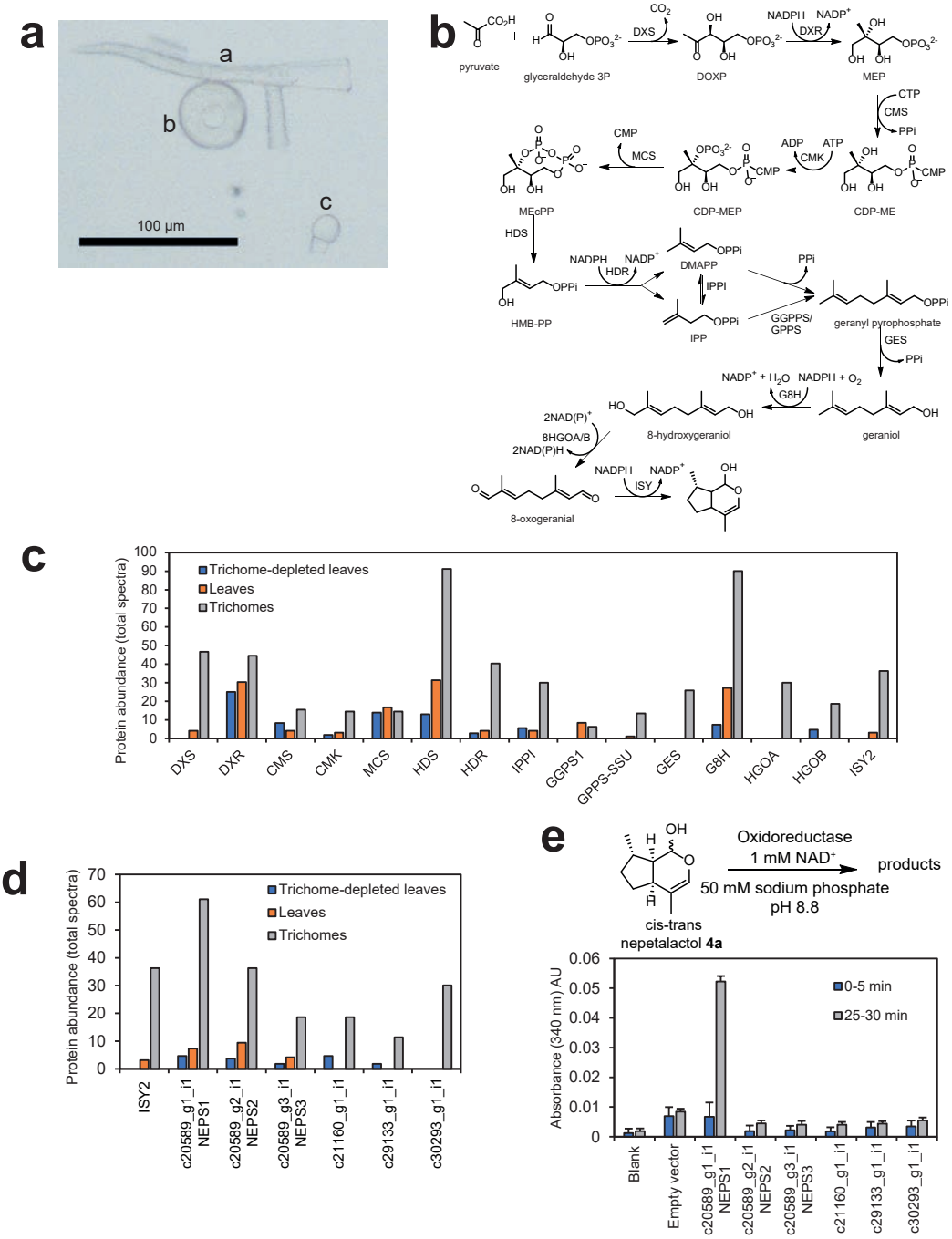

Supplementary Figure 8: Identification of trichome located nepetalactol dehydrogenase. **a**, Isolation of trichomes using dry ice abrasion. Micrograph of isolated trichomes showing different types: non-glandular hairs (a), peltate trichomes (b) and capitate trichomes (c). Trichome isolation was repeated independently twice with similar results but only one sample preparation was used for subsequent proteome analysis. **b**, Isoprenoid 2-*C*-methylerythritol 4-phosphate (MEP) pathway and iridoid biosynthetic pathway. **c**, Enrichment of MEP and iridoid biosynthetic proteins in the trichome measured by shotgun proteomics. All proteins were significantly trichome enriched except for MCS and CMS (trichome compared to trichome-depleted leaves, n=2, Fisher's exact test, $p < 0.05$). **d**, Enrichment of selected oxidoreductases in the trichome. All proteins were significantly trichome enriched (trichome compared to trichome-depleted leaves, n=2, Fisher's exact test, $p < 0.05$). Characterised *N. mussinii* ISY2 included for comparison. **e**, Observation of cis-trans-nepetalactol dehydrogenase activity using UV spectroscopy. Blue bars are averages of A340 over the first 5 mins of reaction (n=10), green bars are averages of A340 over the final 25-31 mins of reaction (n=12). Error bars show one standard deviation from the mean.

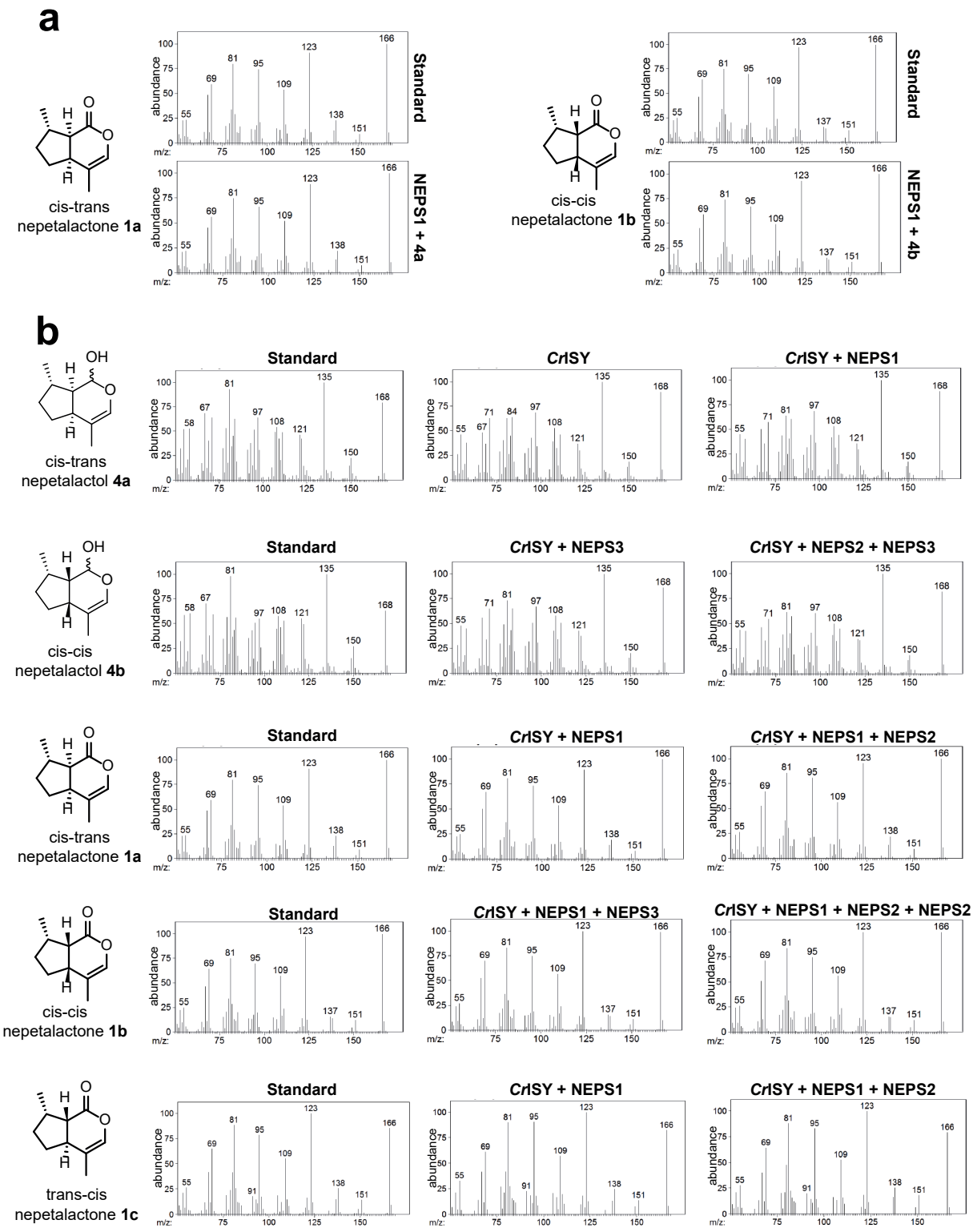

Supplementary Figure 9: Electron ionisation (EI) spectra of compounds from Fig. 3. **a**, Spectra of products from Fig. 3b and c (dehydrogenation reaction). **b**, Spectra of products from Fig. 3d (cascades with NEPS and ISY).

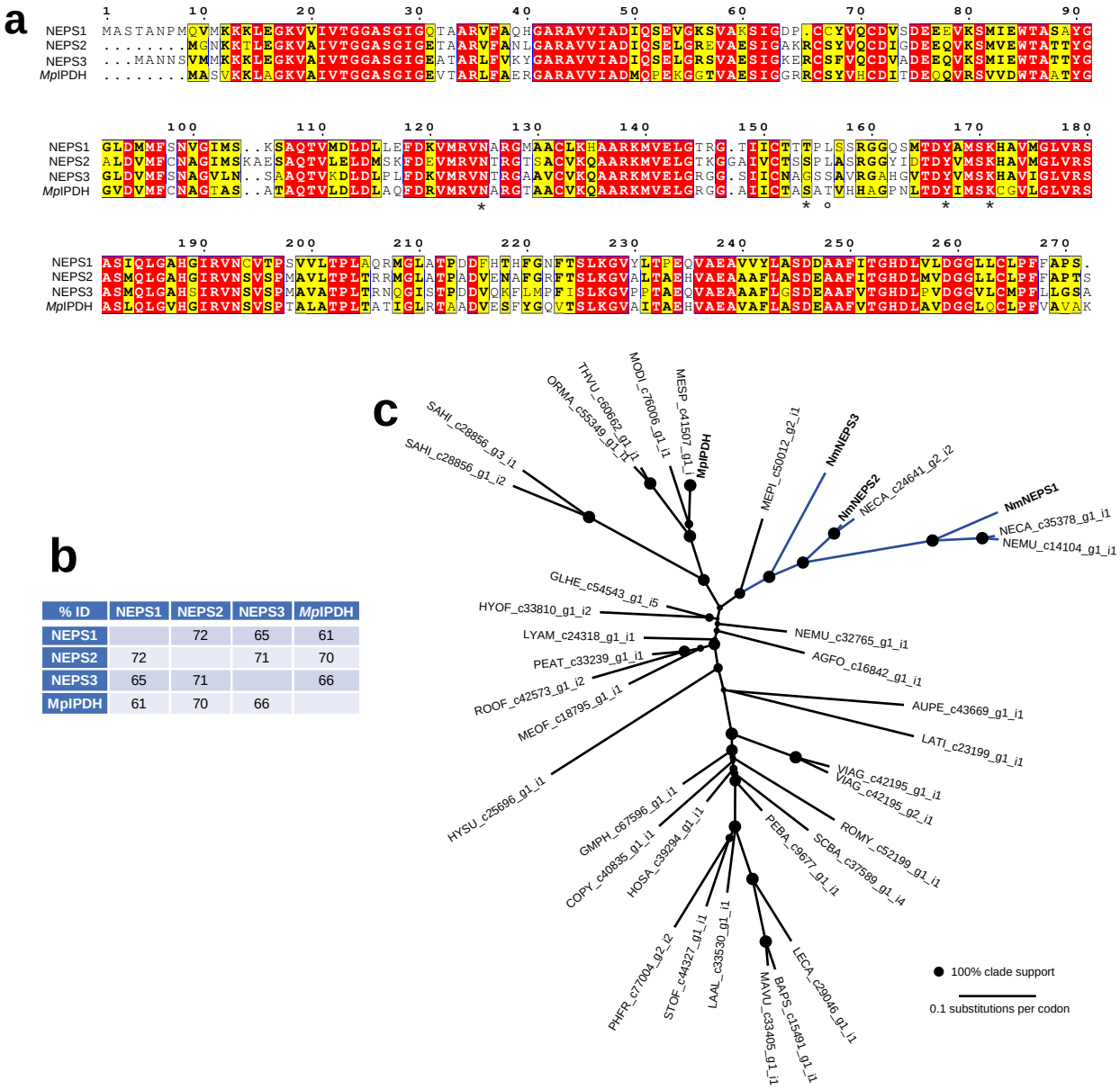

% ID	NEPS1	NEPS2	NEPS3	*Mp*IPDH
NEPS1		72	65	61
NEPS2	72		71	70
NEPS3	65	71		66
MpIPDH	61	70	66	

Supplementary Figure 10: Sequences and phylogeny of NEPS enzymes. **a**, Amino acid sequences of NEPS enzymes cloned from *Nepeta mussinii. Mentha x piperita* isopiperitenol dehydrogenase (*Mp*IPDH) (Uniprot Q5C9I9) included for comparison. Important residues highlighted below the sequence: * are the SDR catalytic tetrad (N-Y-K-T/S) and ° hypothesised to be involved in oxyanion binding in NEPS3. **b**, Sequence identity (%) between NEPS enzymes and *Mp*IPDH. Based on alignment in panel a. **c**, Evolutionary context of NEPS enzymes. NEPS enzymes examined in this study are in bold, as is the previously characterised *Mp*IPDH enzyme. NEPS enzymes appear to locate to a single clade unique to *Nepeta* (blue), implying that these enzymes evolved within the *Nepeta* lineage. Sequences from two cultivars of *Nepeta mussinii* are included: the cultivar used in this study (and in Sherden et al.) and a cultivar used in the Mint Genome Project. Species acronyms: AGFO, *Agastache foeniculum*; AUPE, *Aureolaria pectinata* (outgroup); BAPS, *Ballota pseudodictamnus*; COPY, *Cornutia pyramidata*; GLHE, *Glechoma hederacea*; GMPH, *Gmelina philippensis*; HOSA, *Holmskioldia sanguinea*; HYOF, *Hyssopus officinalis*; HYSU, *Hyptis suaveolens*; LAAL, *Lamium album*; LATI, *Lancea tibetica* (outgroup); LECA, *Leonurus cardiaca*; LYAM, *Lycopus americanus*; MAVU, *Marrubium vulgare*; MEOF, *Melissa officinalis*; MEPI, *Mentha x piperita*; MESP, *Mentha spicata*; MODI, *Monarda didyma*; NECA, *Nepeta cataria*; NEMU, *Nepeta mussinii*; ORMA, *Origanum majorana*; PEAT, *Perovskia atriplicifolia*; PEBA, *Petraeovitex bambusetorium*; PHFR, *Phlomis fruticosa*; ROMY, *Rotheca myricoides*; ROOF, *Rosmarinus officinalis*; SAHI, *Salvia hispanica*; SCBA, *Scutellaria baicalensis*; STOF, *Stachys officinalis*/*Betonica officinalis*; THVU, *Thymus vulgaris*; VIAG, *Vitex agnus-castus*.

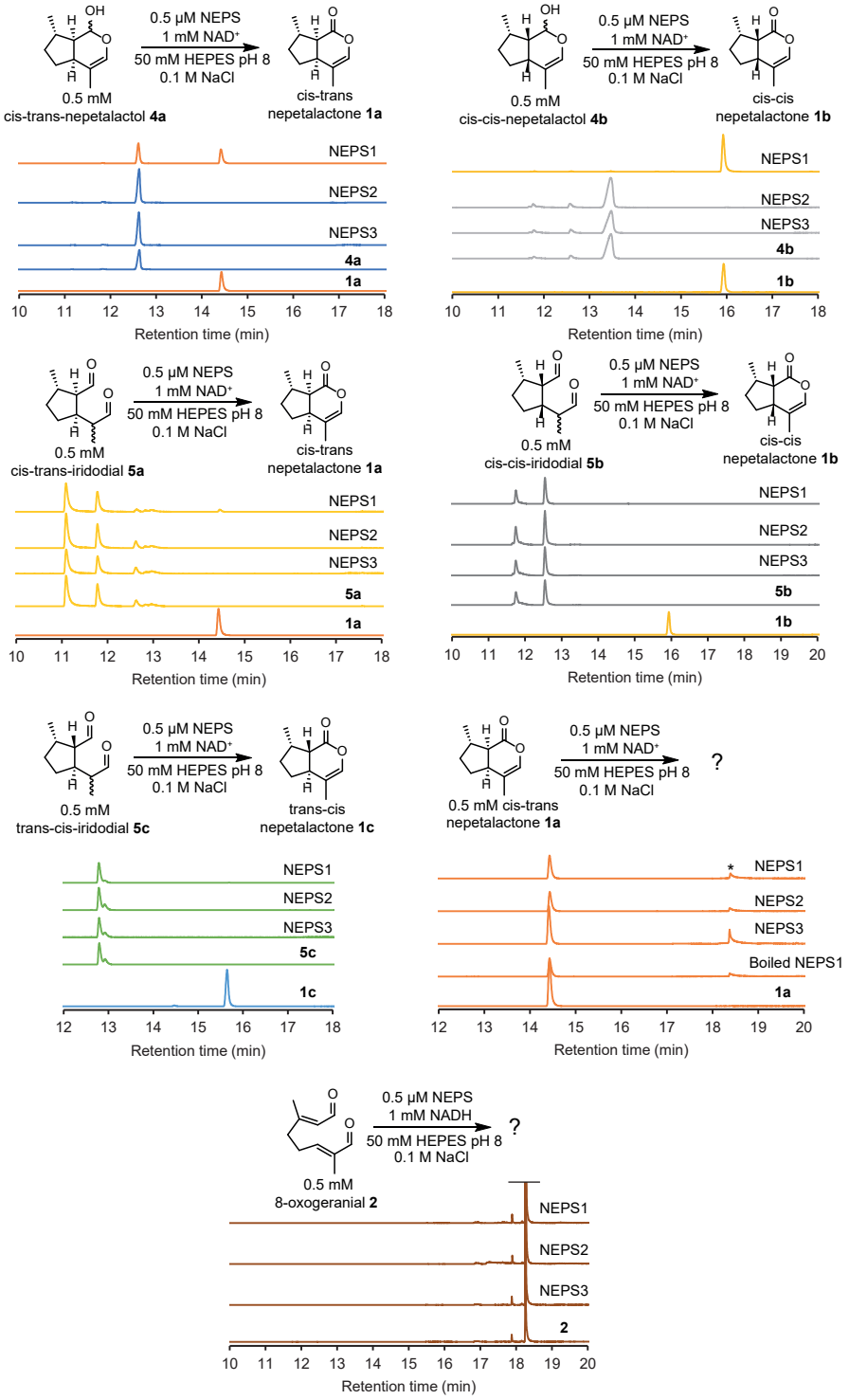

Supplementary Figure 11: Enzyme assays with NEPS enzymes and nepetalactone related substrates. Besides NEPS1 dehydrogenase activity with **4a** and **4b**, no other notable activities are observed (i.e. substrates are not converted into products). NEPS1 appears to produce trace quantities of **1a** with **5a**, however this may be simply conversion of residual **4a** present in the substrate sample. There is also trace formation of nepetalactones **1b** and **1c** by NEPS1 in samples with **5b** and **5c** respectively. An unknown degradation product of **1a** (marked with *) is present in samples using **1a** as the substrate. This is also present in the boiled enzyme control so was not considered to be a NEPS activity. Experiments were conducted once, except for assays with **4a** and **4b**, which were conducted twice with all enzymes, assays with **5a** which were conducted twice with NEPS1 and NEPS2, and assays with **5b** which were conducted twice with NEPS3; all provided similar results. The NEPS activities present here are also supported by activities in cascades (e.g. Fig. 3) and in Supplementary Fig. 12d.

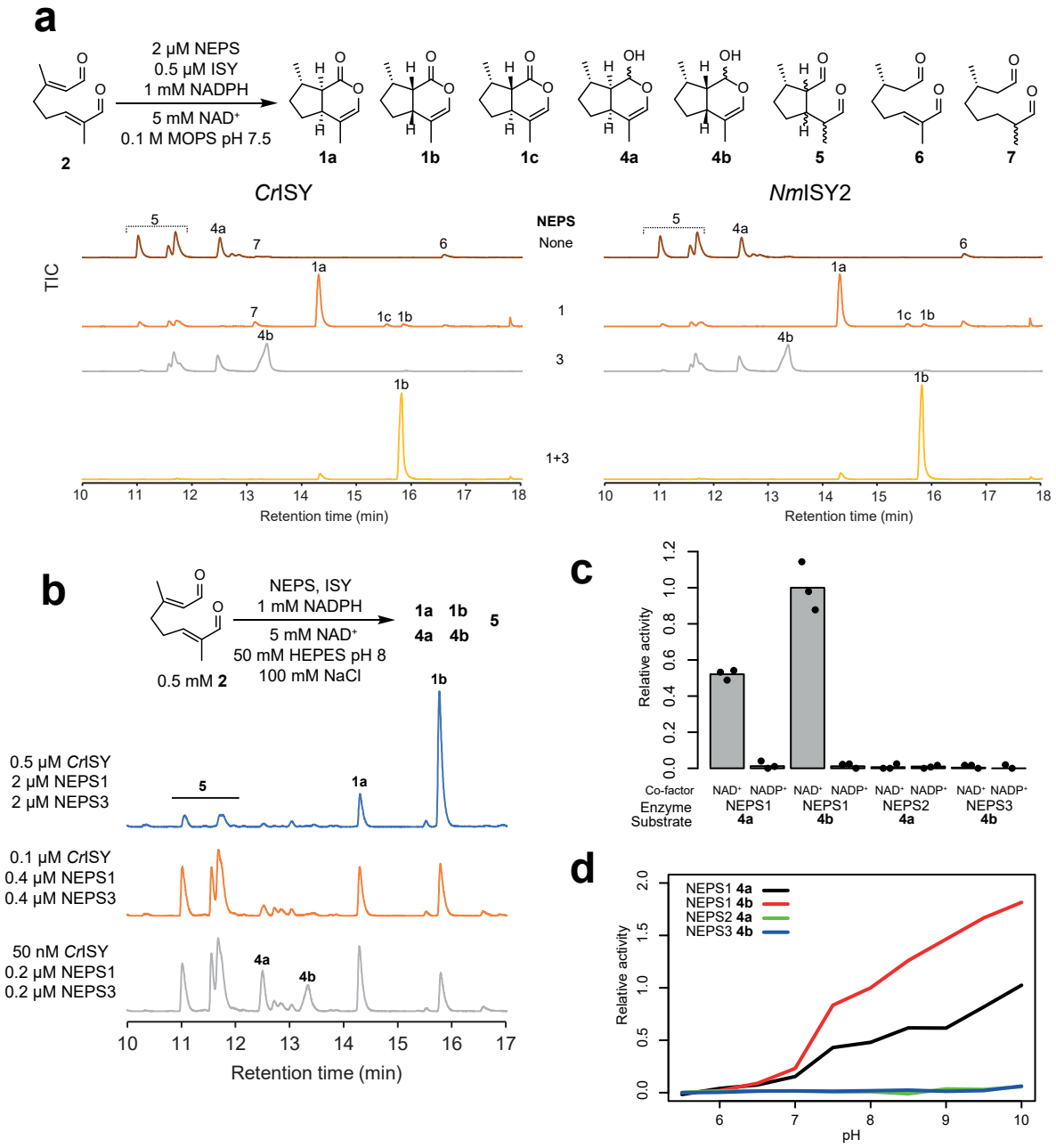

Supplementary Figure 12: Behaviour of NEPS enzymes. **a**. Activity with two distinct ISYs. Cascade reactions with **2**, ISY (*Cr*ISY or *Nm*ISY2), NEPS (1 and/or 3), co-factors and buffer. The behaviour of NEPS enzymes does not appear to be influenced by the ISY employed. The only observable difference between the chromatograms is the trace presence of the double reduction product **7** in reactions with *Cr*ISY. Assays were performed independently twice with similar results. Assays performed under nearly identical conditions also provided similar results (Fig. 3d). **b**. Cascades at different enzyme concentrations. Assays with 2 μM NEPS were performed independently three times with similar results. Assays with 0.4 μM and 0.2 μM NEPS were performed once. **c**. Co-factor dependence of NEPS dehydrogenation activity. Initial rates of NEPS dehydrogenation activities with nepetalactol (**4a** or **4b**) with NAD^+ or $NADP^+$ as co-factor. NEPS1 can oxidise **4a** and **4b** with NAD^+ but cannot utilise $NADP^+$. NEPS2 and NEPS3 demonstrate no dehydrogenation activity with either co-factor. Conditions: 0.1 mM **4a** or **4b**, 1 mM $NAD(P)^+$, 0.25 μM NEPS, 50 mM HEPES pH 8, 100 mM NaCl. Activities normalised to maximum observed rate (NEPS1, **4b**, NAD^+) and depicted as means (grey bars) and individual data points (n = 3, except NEPS3/$NADP^+$ where n=2). **d**. pH dependence of NEPS dehydrogenation activity. NEPS1 oxidation activity is enhanced in high pH conditions. NEPS2 and NEPS3 do not demonstrate notable oxidation activity at any tested pH. Conditions: 0.25 μM NEPS, 0.1 mM **4a** or **4b**, 1 mM NAD^+, 50 mM each HEPES, CHES, MES. Activities normalised to rate for NEPS1, **4b**, pH 8.

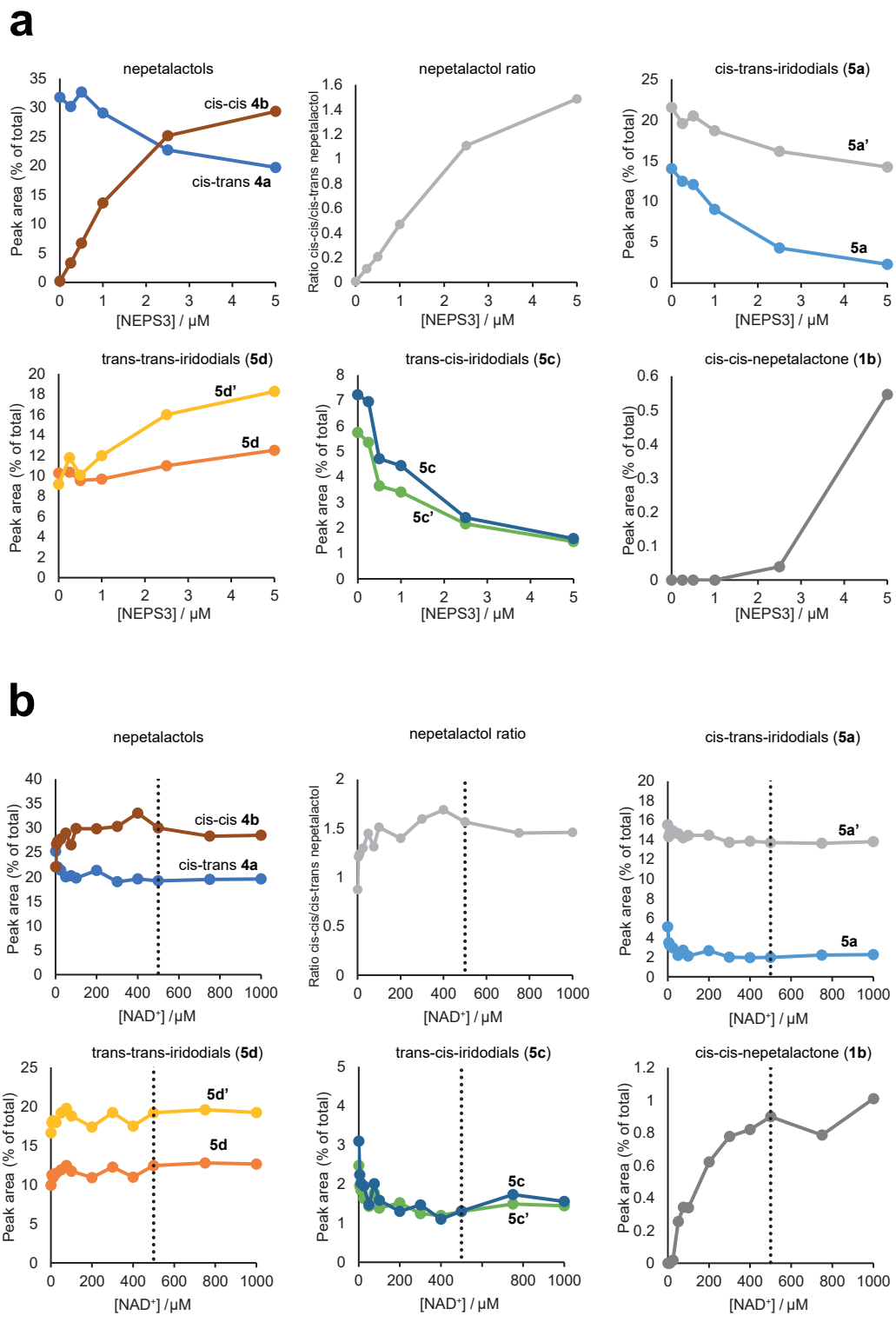

Supplementary Figure 13: Caption and continuation on following page.

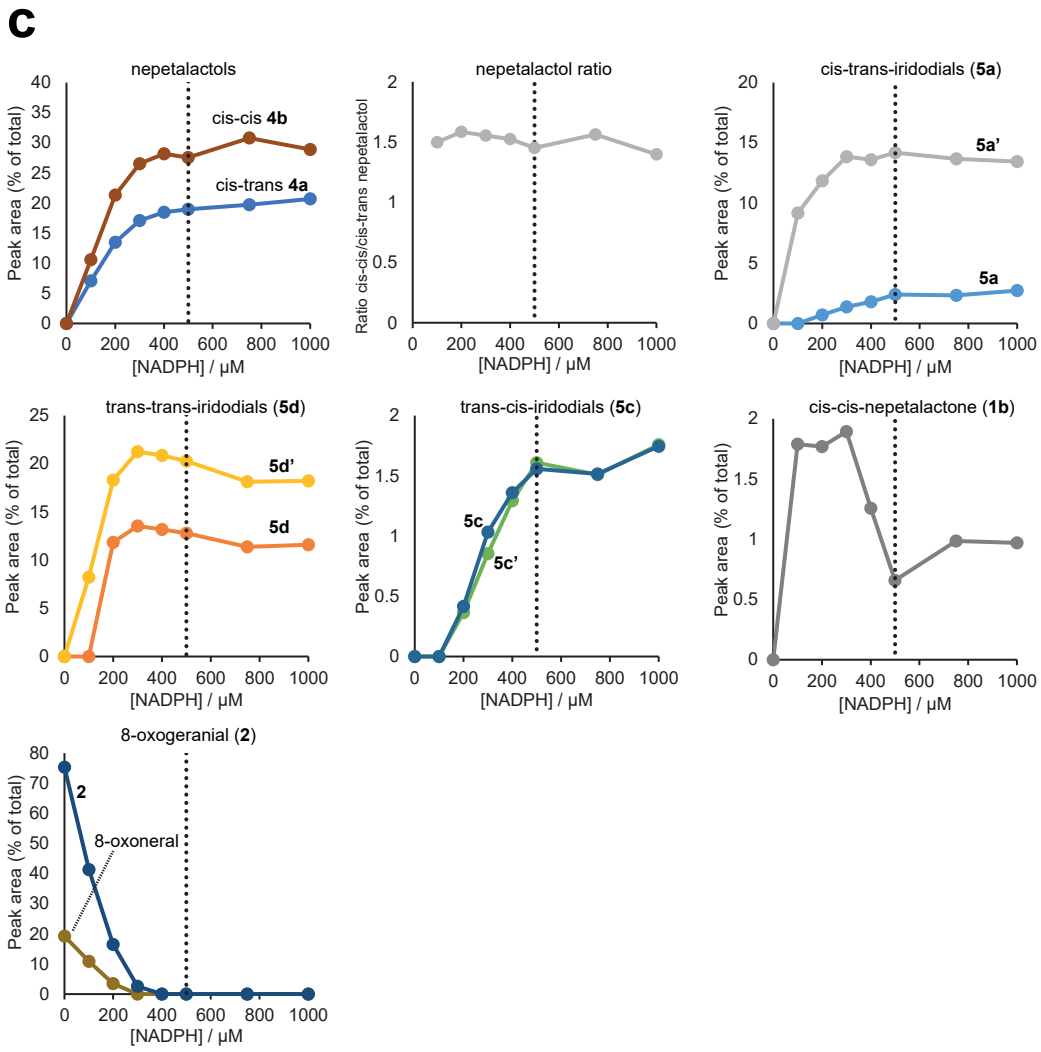

Supplementary Figure 13: Influence of enzyme and co-factor concentrations on NEPS3 activity in conjunction with ISY. **a**, Influence of NEPS3 concentration. As NEPS3 concentration is increased, the proportion of **4b** formed increases. The proportion of **4a**, **5a** and **5c** decrease. At high NEPS3 concentrations, trace formation of cis-cis-nepetalactone is observed. Reactions were conducted with 0.5 µM *Cr*ISY, 0.5 mM **2**, 1 mM NAD^+, 1 mM NADPH, 50 mM HEPES pH 8 and 100 mM NaCl. **b**, Influence of NAD^+ concentration. Reactions contained 0.5 mM **2**, and the equivalent quantity of NAD^+ is represented as a dotted vertical line. If NAD^+ is consumed in the reaction (with equal stoichiometry to **2**), then we would expect maximum conversion at 500 µM and no change beyond this concentration. However, at 50-150 µM [NAD^+] the product proportions reach a maximum, and >200 µM appear relatively stable, most notably proportions of **4a** and **4b**. Only **1b**, a trace oxidation product which requires consumption of NAD^+, shows different behaviour. Furthermore, no remaining substrate **2** was observed in any samples, suggesting full conversion. Between 0-150 µM [NAD^+] the proportions of **4a** and **4b** do appear to change, with **4b** concentration increasing as NAD^+ is supplemented. This data indicates that NAD^+ is not consumed in the NEPS3 catalysed formation of **4b** (i.e. the cyclisation is not oxidoreductive) but its presence does aid the formation of **4b**. It appears to play a strictly catalytic role, for example contributing to the NEPS3 structure. Reactions were conducted as in panel **a** but with varying [NAD^+] and fixed 5 µM NEPS3. **c**, Influence of NADPH concentration. Reactions contained 0.5 mM **2**, and the equivalent stoichiometric quantity of NADPH is represented as a dotted vertical line. If NADPH is consumed in the reaction (with equal stoichiometry to **2**), then we would expect maximum conversion at 500 µM and no change beyond this concentration. This is essentially what is observed. The relative proportions of **4a** and **4b** are unaffected by changing [NADPH], but the overall conversion appears to be limited when [NADPH] < 500 µM. This is also observed in the unreacted substrate **2** at [NADPH] < 500 µM. NADPH appears to be consumed by ISY catalysed reduction, and does not affect NEPS3 cyclisation. Reactions were conducted as in panel **a** but with varying [NADPH] and fixed 5 µM NEPS3. Product peak areas are represented as percentage product proportions, obtained by dividing product TIC peak area by total product peak areas. Product peak areas are not normalised by standard curves so do not represent absolute concentrations. Note that peaks of **5a'** and **5d'** overlap in the GC method—peak areas for these compounds were measured as a split peak (i.e. both to baseline) and not as a peak shoulder.

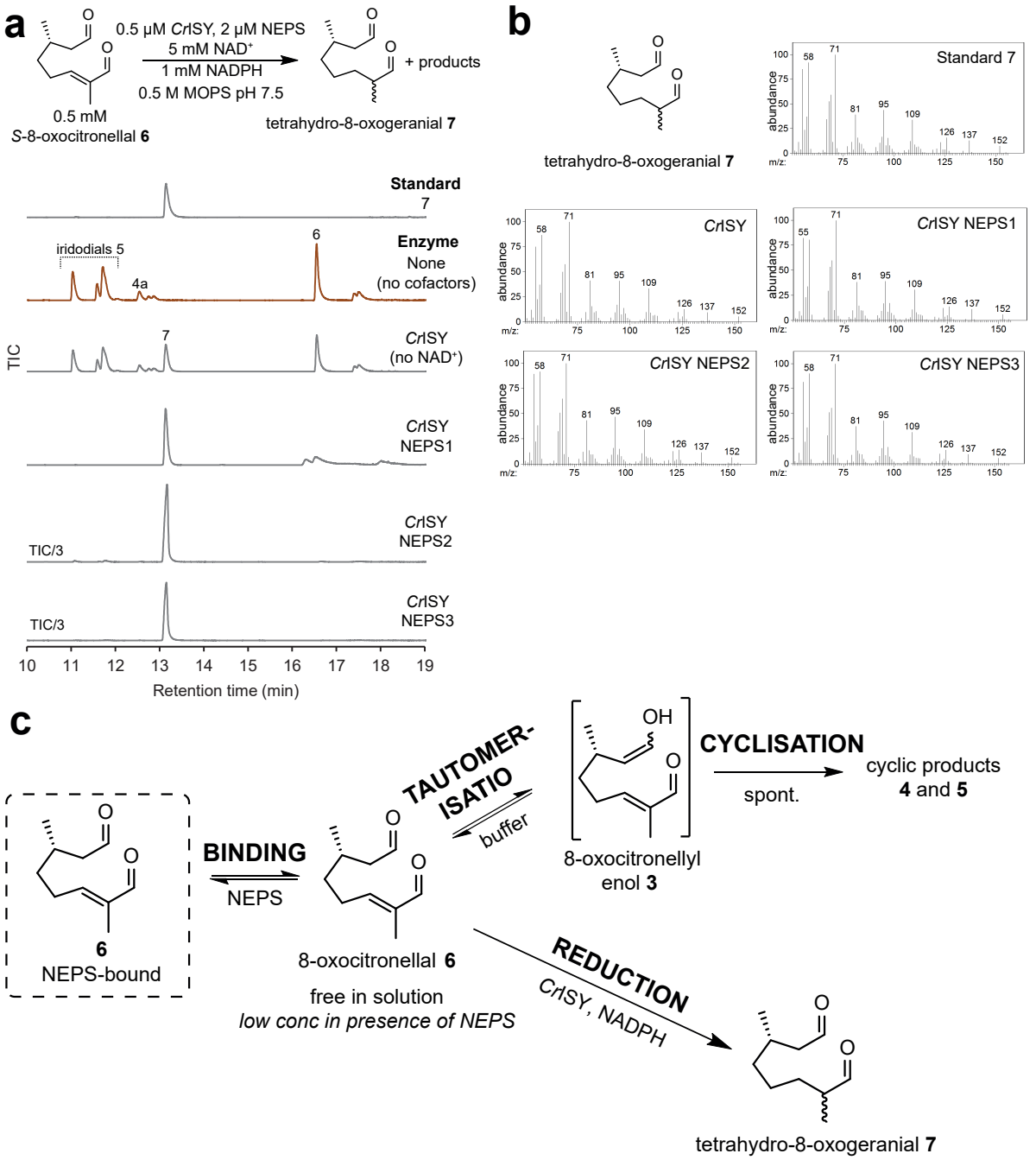

Supplementary Figure 14: Reaction with 8-oxocitronellal **6**, *Cr*ISY and NEPS enzymes. **a**, GC-MS TICs of reactions with **6**, *Cr*ISY, NEPS, cofactors and 0.5 M MOPS pH 7.5. The production of tetrahydro-8-oxogeranial **7** when both *Cr*ISY and NEPS are present is notable. TIC abundances for *Cr*ISY+NEPS2 and *Cr*ISY+NEPS3 have been reduced threefold. **b**, EI spectra of compound panel a compound **7** in different reactions. **c**, Scheme of proposed processes occurring in cascades with **6**, *Cr*ISY and NEPS. When no enzymes are present, **6** undergoes buffer catalysed tautomerisation and cyclisation to form **4a** and iridodials **5** (panel a, second chromatogram from top). *Cr*ISY reduces **6** to tetrahydro-8-oxogeranial **7**. This reduction is in competition with the spontaneous tautomerisation/cyclisation—the **6** that *Cr*ISY is not able to reduce will undergo tautomerisation/cyclisation (panel a, third chromatogram from top). When both *Cr*ISY and NEPS enzymes are added, the tautomerisation/cyclisation process appears to be minimised, and **7** accumulates (panel a, bottom three chromatograms). To account for this, we hypothesise that NEPS are reversibly binding **6**, reducing the concentration of free **6** in solution. *Cr*ISY is then able to reduce all the free **6** into **7**, depleting **6** before it undergoes tautomerisation/cyclisation. In reactions with NEPS2 or 3 this process appears to ultimately convert all **6** into **7** (panel a, bottom two chromatograms). A crucial aspect of this process is that NEPS enzymes appear to be binding **6** without turning it over. This supports the notion that the enol **3** and not **6** is the key substrate for NEPS enzymes. The assay was performed independently twice with similar results.

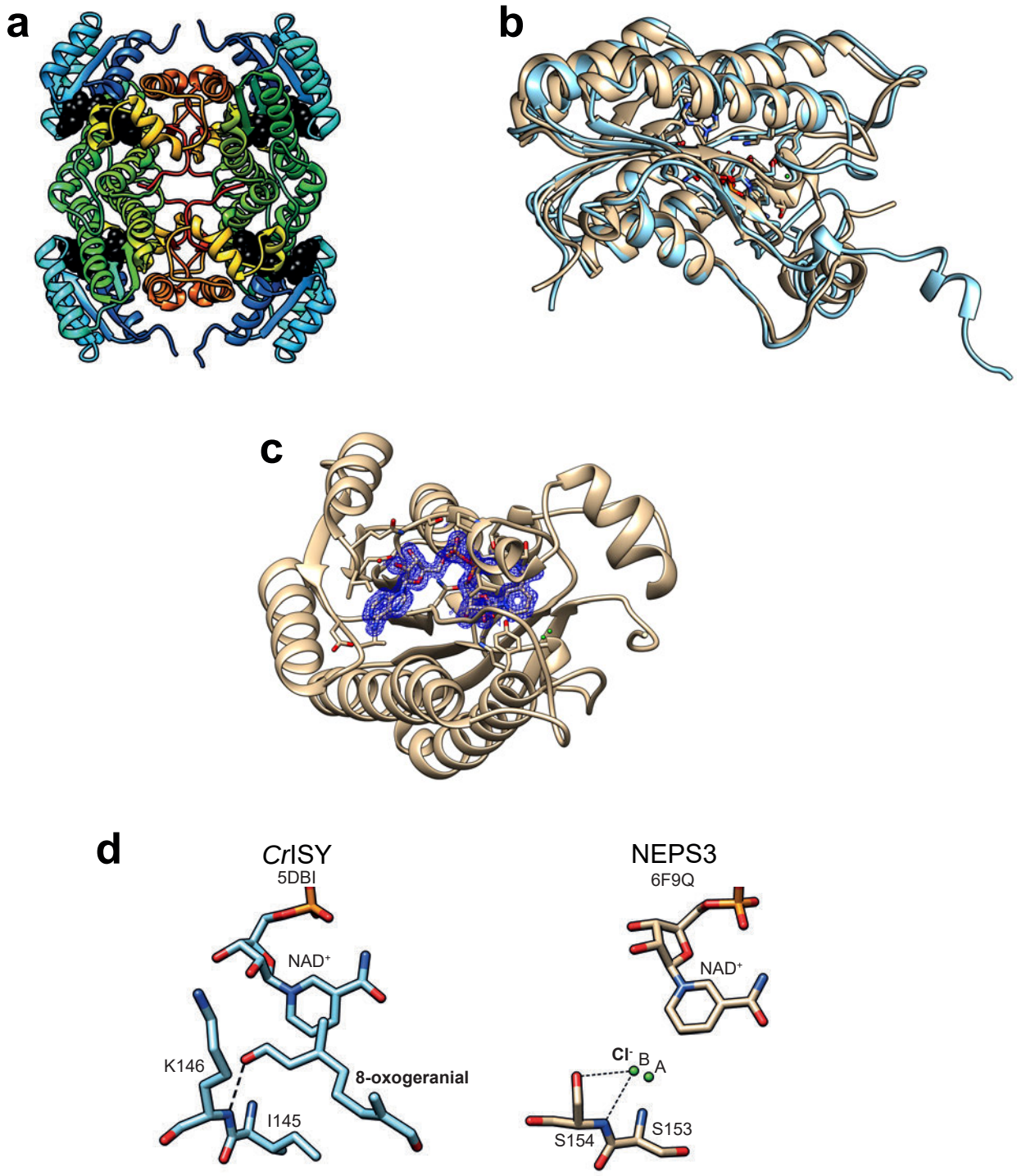

Supplementary Figure 15: Structure of NEPS3 (6F9Q). **a**, NEPS3 tetramer structure. Subunit main-chain ribbons are rainbow coloured from N-termini (blue) to C-termini (red). NAD^+ co-factors depicted as black spheres. **b**, NEPS3 subunit A structure aligned to secoisolariciresinol dehydrogenase (2BGL). NEPS3 depicted as light brown ribbons, secoisolariciresinol dehydrogenase depicted as cyan ribbons. Active site residues and NAD^+ depicted as sticks. The two enzymes have 42% sequence identity. **c**, NEPS3 subunit A main chain depicted as ribbons, with NAD^+ depicted as sticks. The 1.4 Å resolution electron density for the cofactor only (blue mesh, 2mFo-DFc, contoured at 1 σ) is also shown. **d**, Comparison of *Cr*ISY substrate binding site (5DBI) and NEPS3 chloride binding site. We hypothesise that the chloride occupies an oxyanion site (S154), analogous to the site on *Cr*ISY (K146). The chloride in NEPS3 is discreetly disordered and was refined in two positions A and B each with 50% occupancy. The chloride position B has a lower B-factor than position A in all four subunits. Due to this, it appears that position B is the major contributor to the electron density.

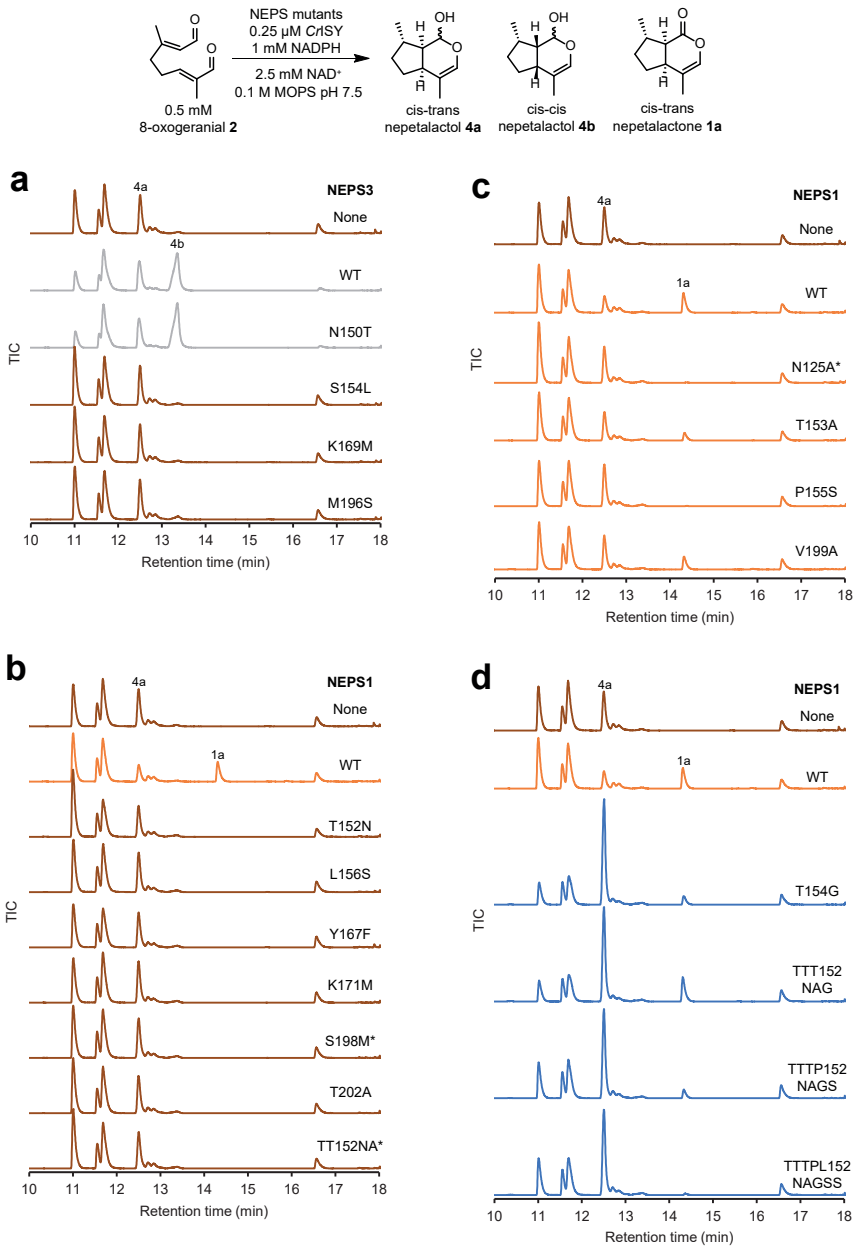

Supplementary Figure 16: Screen of NEPS1 and NEPS3 mutants. NEPS1 and NEPS3 mutants were grown in 10 mL cultures, partially purified and assayed. The assays were conducted with 0.5 mM 8-oxogeranial **2**, 0.25 µM *Cr*ISY, 2.5 mM NAD^+, 1 mM NADPH and 0.1 M MOPS pH 7.5. Reactions were incubated for 8 h at 30 °C. NEPS concentrations were approximately 2 µM (total protein including impurities) based on absorbance at 280 nm. **a**, NEPS3 variants with soluble expression. N150T has maintained NEPS3 activity. S154L, K169M and M196S demonstrate low or no detectable formation of **4b**. Variants A151T, G152T, S153P, Y165F had no detectable soluble expression. **b**, NEPS1 variants demonstrating no detectable formation of **1a**: T152N, L156S, Y176F, K171M, T202A. Variants labelled * (TT152NA, S198M) demonstrated poor soluble expression and thus low conversions may be a result of low NEPS concentrations and not simply activity. **c**, NEPS1 variants demonstrating detectable formation of cis-trans-nepetalactone **1a**. Variants T153A and V199A demonstrated reasonable conversions. Variants N125A and P155S catalysed trace but detectable formation of **1a**. N125A demonstrated poor soluble expression/purification and thus low conversions may be a result of low NEPS concentrations and not simply activity. **d**, NEPS1 variants containing the T154G substitution. All variants containing T154G showed increased formation of **4a** compared to WT. T154G and TTT152NAG demonstrated the greatest cyclase activity (formation of **4a** and decrease in iridodials **5**), whilst maintaining reasonable dehydrogenase activity (evidenced by presence of **1a**). TTTP152NAGS and TTTPL152NAGSS showed greater formation of **4a** than WT but only trace dehydrogenase activity (**1a**). T154G is examined further in Fig. 6, Supplementary Fig. 17 and Supplementary Table 2. The screening experiments presented here were performed independently twice with similar results.

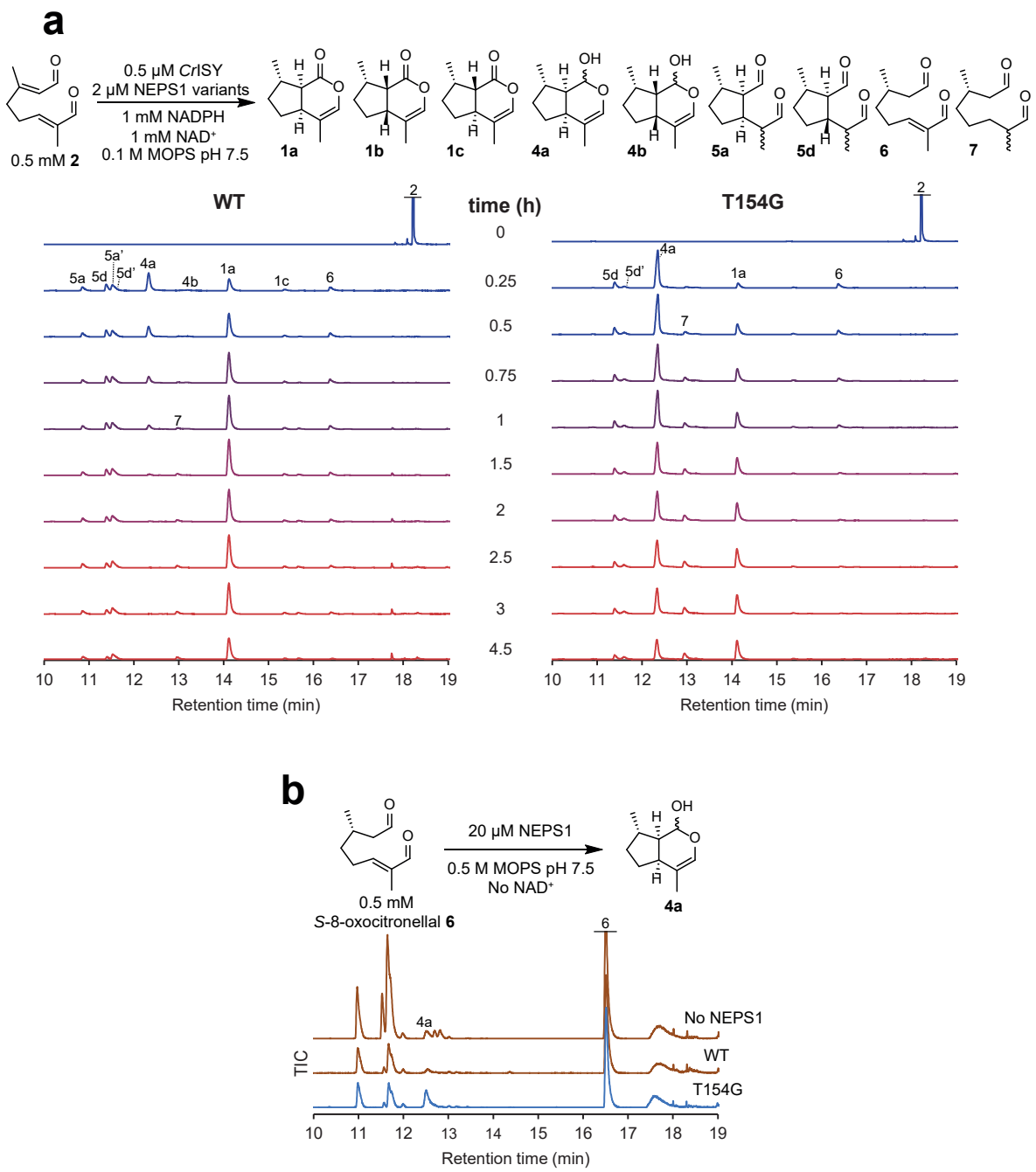

Supplementary Figure 17: Behaviour of NEPS1-T154G variant. **a**, Time course of coupled assay with **2**, ISY and NEPS1 WT or T154G, presented as GC-MS TICs. Peak areas of **4a** and **1a** described in Fig. 6b. Full time courses were performed once, but conversions after 3 h were performed independently twice with similar results. Kinetic analysis of NEPS-T154G can be found in Supplementary Table 2. **b**, Cyclase activity of NEPS1 investigated with **6**. In the absence of additional co-factor, NEPS1 does not appear to detectably form **4a** in the presence of **6** and buffer at greater than background levels. In contrast, NEPS1-T154G forms **4a** at greater than background levels in the same conditions. Experiments were performed once, but T154G improved cyclisation activity is also supported by reduction of **5a** in panel a.